

Evaluation of Pebble Scanning Strategies for Fuel Qualification by Simple Simulated Radiography

Grant W. Helmreich¹, Daniel R. Brown², and Brandon Blamer²

¹*Oak Ridge National Laboratory, Oak Ridge, TN 37831, United States*

²*X-energy LLC, 801 Thompson Ave., MD 20852, United States*

This manuscript has been authored by UT-Battelle, LLC, under contract DE-AC05-00OR22725 with the US Department of Energy (DOE). The US government retains and the publisher, by accepting the article for publication, acknowledges that the US government retains a nonexclusive, paid-up, irrevocable, worldwide license to publish or reproduce the published form of this manuscript, or allow others to do so, for US government purposes. DOE will provide public access to these results of federally sponsored research in accordance with the DOE Public Access Plan (<http://energy.gov/downloads/doe-public-access-plan>).

Abstract

Reactor designs using tristructural-isotropic (TRISO) particles in pebble fuel forms have been developed in multiple programs and are now being designed and deployed by several companies around the world. Fuel pebbles for these designs commonly contain an inner fueled zone packed with TRISO particles and a fuel-free zone on the surface of the pebble to protect the particles within. Therefore, qualification of pebbles for use in a reactor commonly requires determination that there are no TRISO particles within a given minimum distance to the pebble surface. This determination may be made non-destructively by pebble radiography, in which a series of x-ray projections of the pebble are acquired. In this work, a method to create and image representative digital pebbles was developed to allow for rapid testing of various pebble radiography strategies to evaluate their effectiveness in detecting escapee particles. Using this method, imaging strategies in two and three dimensions were tested with fixed and adaptive angular distributions. It was found that an adaptive two-dimensional pebble scanning strategy was the most effective for fuel pebble qualification.

1 Introduction

Tristructural-isotropic (TRISO) particle-based nuclear fuels are technologically mature, with demonstrated in-reactor performance. As such, many reactor designs using TRISO particles are currently under development, and many of these designs use TRISO particles in the form of spherical graphite matrix pebbles [1]. The specific geometry of these pebbles varies with reactor design, but a common feature is the presence of a fuel-free zone of graphite matrix surrounding a spherical fuel core which contains thousands of TRISO particles embedded in graphite matrix. The fuel-free zone protects TRISO particles within the pebble from mechanical damage and serves as a final containment layer for fission products generated during irradiation [2]. Typically, the fuel-free zone is specified to be within a range of tolerable thickness (e.g., 4–6 mm thick for a pebble that is nominally 60 mm in diameter).

Determination of fuel-free zone thickness on an industrial scale poses a significant challenge to rapidly measure a three-dimensional (3D) property while avoiding destructive analysis of many pebbles. The thickness of the fuel-free zone in 3D may be determined destructively by serial sectioning or nondestructively by x-ray computed tomography (XCT) [3, 4, 5, 6]; however, these methods are time consuming. In the best case, if fuel-free zone thickness is treated as a variable property which follows a

normal statistical distribution within a population of pebbles, then hundreds of pebbles from each lot would likely need to be sampled to sufficiently define the statistical distribution. In the alternate case, if insufficient fuel-free zone thickness is treated as an attribute property with some maximum acceptable defect fraction, then samples of thousands to tens of thousands of pebbles may be required to reach the required confidence value in the acceptable defect fraction [4]. Determining which statistical treatment is correct depends on the basis with which the fuel-free zone is being specified. If the intent is to limit variations in minimum fuel-free zone thickness due to the fuel core and the pebble not being concentric, then treatment as a variable property may be justified. However, if the intent is to prevent using pebbles with escaped particles broken from the fuel core and embedded in the fuel-free zone during fabrication, then either each pebble must be inspected, or escaped particles must be treated as an attribute property.

Industrial XCT systems offer significantly faster sample scanning the laboratory scale systems by using higher power sources, typically at lower resolutions [8, 9]. However, a faster approach which has been previously reported is to use a series of x-ray radiographs taken of each pebble at distributed angles to estimate the centroids and radii of the fuel core and full pebble [5]. This approach is potentially much faster than full XCT imaging, but it entails an inherent increase in the volume of blind spots within the pebble which are not directly imaged and which may contain escaped particles [6]. If sufficient geometric data can be generated from each pebble in a very rapid scan, then this method may be scalable to qualify each pebble produced at an industrial facility rather than relying on statistical sampling. The question becomes how many radiographs are required per pebble for a given confidence value in the fuel-free zone thickness. This question is addressed herein by simulated radiography of digital pebbles. This approach has key advantages over manual pebble fabrication and imaging, as large numbers of unique digital pebbles with varying properties may be rapidly and inexpensively generated and imaged. Simulation of TRISO-bearing pebbles has been successfully applied in the past [10], but the focus of this work is not on the development of high-fidelity simulation methods, but rather on the application of a relatively simple simulation approach to evaluate pebble scanning strategies for fuel qualification.

2 Digital Pebble Generation and Radiography

2.1 Creation of Digital Pebbles

The algorithm for creation of digital pebbles was based on knowledge of typical particle distributions and fuel core shapes within pebbles as obtained from XCT imaging. Pebbles typically feature an approximately spherical fuel core, with TRISO particles approximately evenly spaced in a tightly packed array with a given nearest-neighbor distance [3]. To recreate these features in a digital pebble, kernels were initially modeled in a close-packed array with a user-defined nearest-neighbor distance. The position of each of these kernels was shifted in a random direction by (1) a distance randomly determined from the normal distribution and (2) a user-defined standard deviation of the nearest-neighbor distance. This resulted in a pseudo-close-packed array of kernels filling a cubic digital matrix. In this work, TRISO particles are represented only by their kernels since the TRISO coating layers are generally indistinguishable from the surrounding graphite matrix in pebble radiographs [3]. While the distribution of particle nearest-neighbor distances may not be precisely normal [4], this approximation is reasonable given the goal of establishing a simple simulation method to test pebble scanning strategies.

The next step was to define an approximately spherical fuel core. The fuel core began as an ellipsoid of three user-defined principal radii at a given orientation. This ellipsoid was modified by applying user-defined facets to its surface. Finally, the centroid of the fuel core was shifted from the center of the cubic matrix to create an offset between the fuel core and pebble centroids. Once the fuel shape was fully defined,

all kernels with a centroid outside the fuel core were removed. The parameters defining the shape of the fuel core may either be input directly or generated randomly. Direct input of fuel core shape parameters may be useful for studying the impact of individual deviations (e.g., a large singular facet), while random parameter generation allowed for more realistic shapes featuring a range of minor deviations from sphericity, such as several facets of varying depth, slight overall eccentricity, and a slightly shifted centroid in a single pebble. The final step was to define the surface of the pebble itself. Since pebbles are machined to a high degree of sphericity, the pebble surface was defined as a sphere of a given radius centered in the middle of the cubic matrix. A two-dimensional (2D) representation of the entire algorithm for the generation of digital pebbles is shown in **Fig 1**.

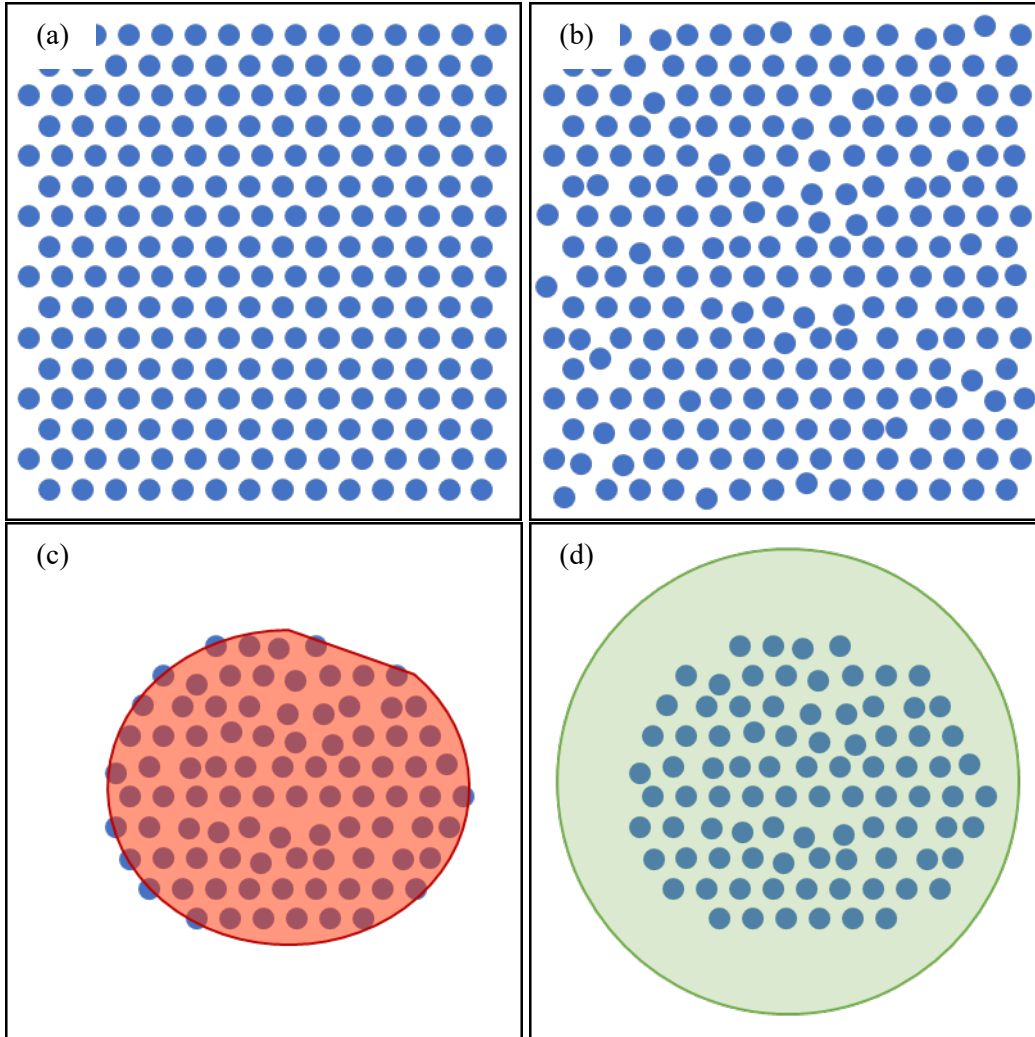


Fig 1. 2D representation of digital pebble creation algorithm. TRISO kernels were initialized in a close-packed array (a) and then randomly shifted (b). A fuel core ellipsoid was defined, kernels outside the fuel core were removed (c), and then a spherical pebble surface was defined (d). Note: not to scale.

A set of 100 pebbles was generated using this algorithm with the parameters given in **Table 1**. The particle distribution parameters used were based on XCT data of actual pebbles [3], while the pebble defects of variations in fuel core diameter, fuel core/pebble centroid offsets, and fuel core facet depths were based on estimates of the worst case results of the manufacturing process. While the precise number of particles in each pebble was determined by random variation in fuel core shape, pebbles in this work generally

contained ~16,000–17,000 particles each with these parameters. This set of digital pebbles was used for all analyses performed herein.

Table 1. Parameters used for random generation of test population of 100 digital pebbles.

Two-sided Gaussian parameters	Minimum (mm)	Mean (mm)	Std. Dev. (mm)
Nearest-neighbor distance	n/a	1.75	0.3
Fuel core ellipsoid axis lengths	n/a	50	0.5
Fuel core/pebble centroid offset	n/a	0	0.5
Fuel core facet depth	0	3	1
One-sided Gaussian parameters	Minimum		Std. Dev.
Number of facets	0		1
Fixed parameters			
Voxel size	0.1 mm		
Pebble diameter	60 mm		
Kernel diameter	0.425 mm		

2.2 Simulated Radiography of Digital Pebbles

After a digital pebble was created, simulated radiographs were generated for analysis. Pebbles were imaged at given angles by projecting the 3D matrix onto a 2D array at that angle. A simplified approach similar to Maximum Intensity Projection was applied in which each pixel in the simulated pseudo-radiograph was determined by the highest value voxel projected onto it from the 3D matrix at the given angle with a ranking order of kernel voxels, pebble voxels, and then other voxels. This ranking accurately recreated actual radiographs of pebbles, as shown in **Fig. 2**.

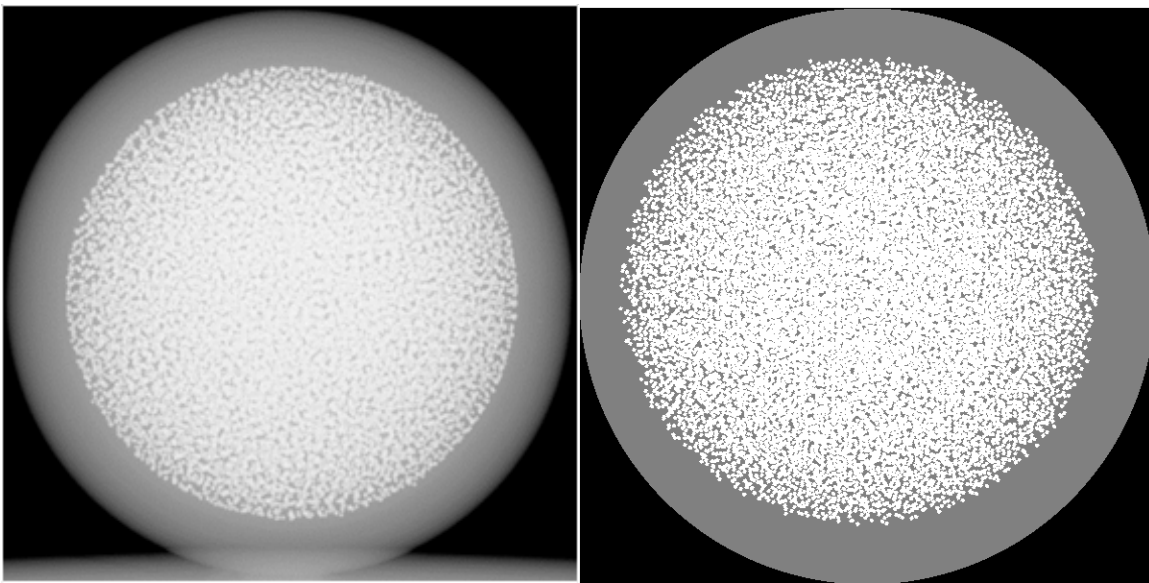


Fig. 2. Inverted radiograph of an actual pebble (left) and simulated radiograph of a digital pebble (right).

This algorithm for simulated radiography is slightly simplified from the typical case, as it assumes a parallel beam rather than the cone beam commonly used in x-ray radiography systems; however, it has previously been shown that blind spots within pebble radiographs are minimized by maximizing the source-to-sample distance, which approximates a parallel beam [6]. As such, it is reasonable to assume that any industrial pebble qualification system will either use a parallel beam source or operate a cone beam source with parameters to approximate a parallel beam.

3 Determination of Variable Fuel-Free Zone Thickness from Radiograph Sets

High-quality reconstruction of radiograph image sets into 3D tomograms requires large numbers of radiographs; however, sets of as few as two radiographs may be used to estimate the distribution of fuel-free zone thickness around each digital pebble. First, the geometric centroid of the fuel core in each radiograph was determined based on the convex hull of the kernel mask, as shown in **Fig. 3**.

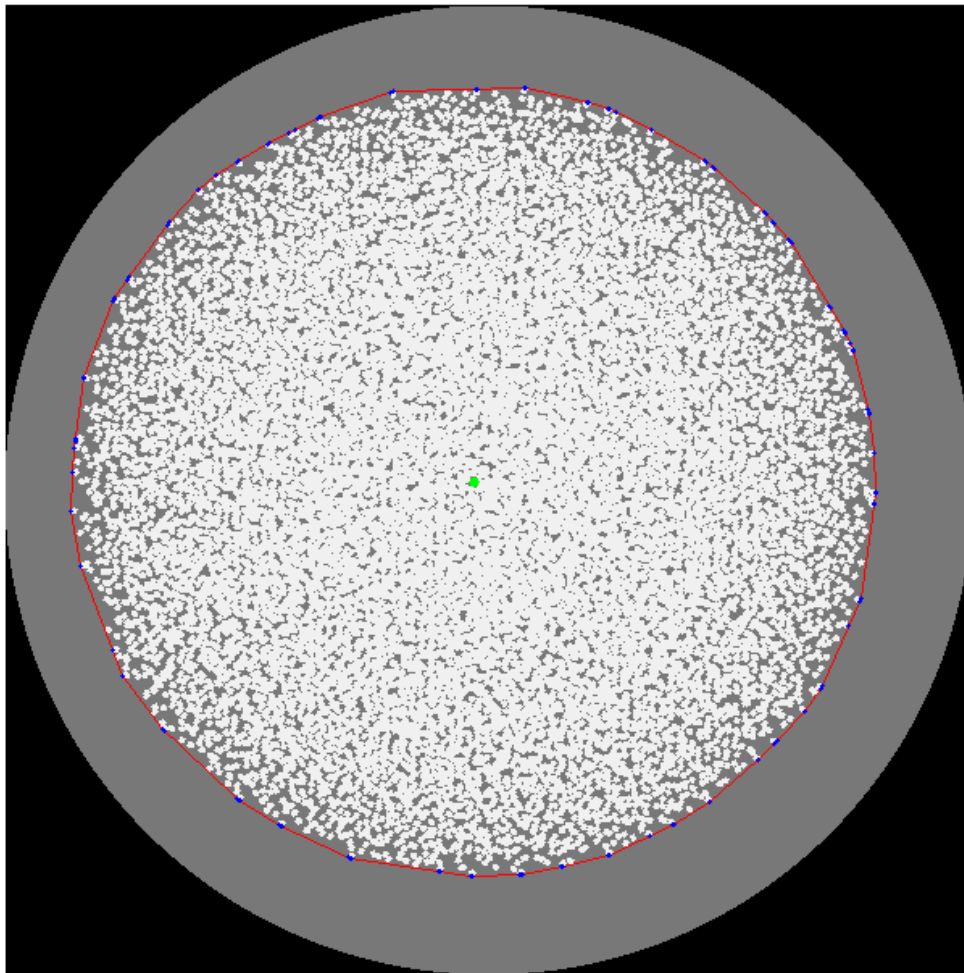


Fig. 3. Simulated radiograph of graphite matrix (grey) and kernels (white) with the convex hull of the fuel core (red), fuel core surface pixels (blue), and the fuel core centroid (green) marked.

Assuming a spherical fuel core, the centroid x_i, y_i in radiograph i taken at a polar angle θ and azimuthal angle φ may be found from the true centroid of the fuel core x_c, y_c, z_c using Equation 1. Since each radiograph produces a system of two linear equations relating the radiograph centroids to the fuel core centroid, with two or more radiographs, the fuel core centroid may be calculated based on a least-squares fit to the system

of linear equations. This method was used for each set of radiographs to generate an initial estimate of the fuel core centroid.

$$\begin{bmatrix} x_i \\ y_i \end{bmatrix} = \begin{bmatrix} \cos(\varphi_i) & \sin(\varphi_i) & 0 \\ \cos(\theta_i) \cdot \sin(\varphi_i) & \cos(\theta_i) \cdot \cos(\varphi_i) & \sin(\theta_i) \end{bmatrix} \begin{bmatrix} x_c \\ y_c \\ z_c \end{bmatrix} \quad (1)$$

Next, pixels on the surface of the fuel core were identified in each radiograph by selecting only those present in both the kernel mask and the convex hull, as shown in **Fig. 3**. Each of these surface pixels in the radiograph represents a line passing through a voxel on the surface of the fuel core, and each voxel on that line must satisfy Equation 1). This results in an underdetermined system of equations for determination of the true position of the surface voxel, so an additional constraint was imposed: that the point on the surface of the fuel core should be at the shortest possible distance from the fuel core centroid. With this additional constraint, each surface pixel identified in each radiograph could be converted into a 3D coordinate on the fuel core surface. As shown in **Fig. 4**, for a digital pebble imaged at six angles in 3D space, the calculated geometric positions of the surface points identified in each radiograph align closely with the actual fuel core surface. The set of these points were fit to an ellipsoid to model the apparent 3D structure of the fuel core. This process was repeated to refine the initial estimate of the fuel core centroid without the assumption of sphericity.

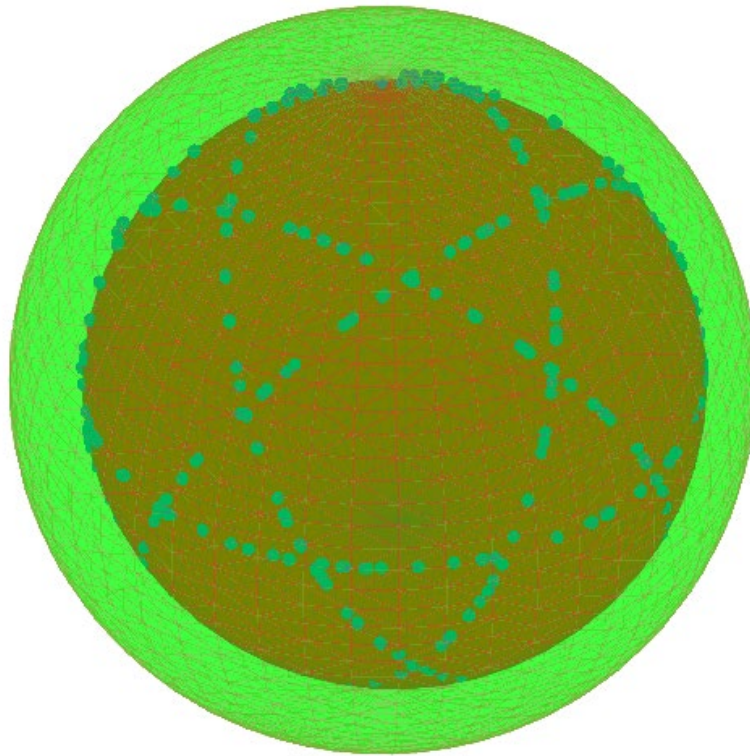


Fig. 4. Pebble (green) with fuel core (red) and the set of fuel core surface points identified from radiograph projections (blue) used to fit an ellipsoid to the fuel core.

Once the fuel core was modeled based on each radiograph set, the apparent fuel-free zone thicknesses around the fuel core was characterized by calculating the distance between the surface of the calculated fuel core ellipsoid and the pebble surface at a set of 1,200 equidistributed spherical angles to generate mean, minimum, and maximum fuel-free zone thicknesses. These values were compared to the exact values

generated directly from each digital pebble. This process was tested on the set of randomly generated pebbles described in Section 2.1 with varying numbers of radiographs per imaging set distributed evenly in either 2D (rotating on one axis) or 3D (rotating on two axes).

As shown in **Fig. 5**, the mean error in the mean fuel-free zone thickness for each imaging strategy tested was negative, indicating that the calculated fuel-free zone thickness was on average slightly smaller than the true value. This bias was due to the fitting of smooth ellipsoids to faceted fuel cores, which will naturally tend to extend the fuel core surface out over the facets. The magnitude of the mean and the standard deviation of the error in the mean fuel-free zone thickness decreased slightly with increasing numbers of radiographs per imaging set, and there was not a significant difference in results between the planar and 3D distribution of radiographs.

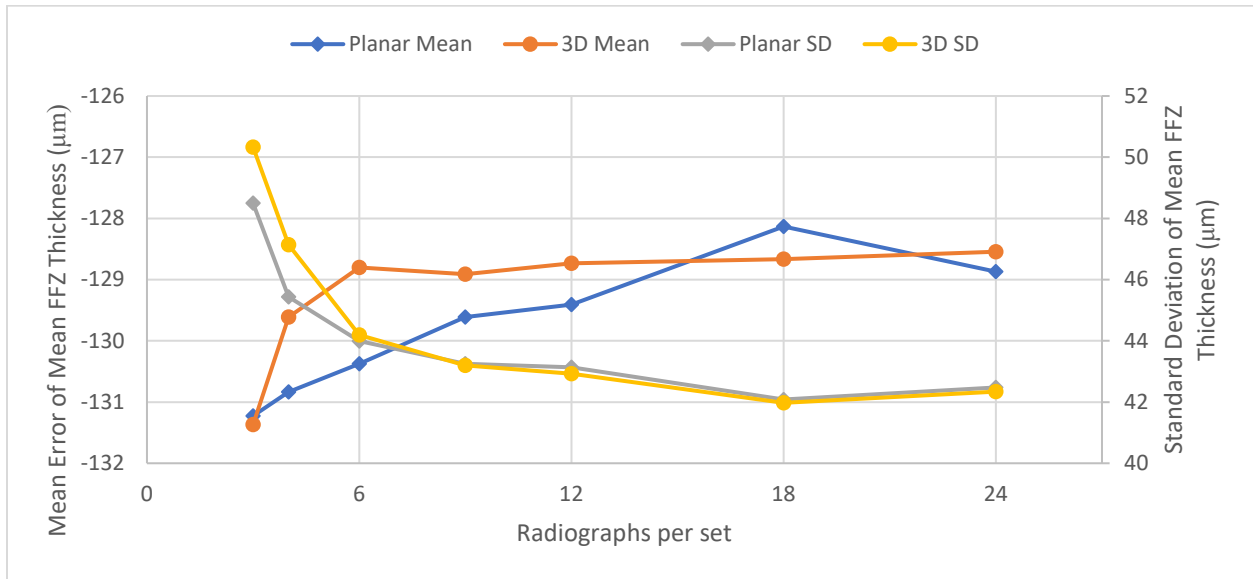


Fig. 5. Mean and standard deviation of error in mean fuel-free zone (FFZ) thickness for varying numbers of radiographs per set in both planar and 3D configurations.

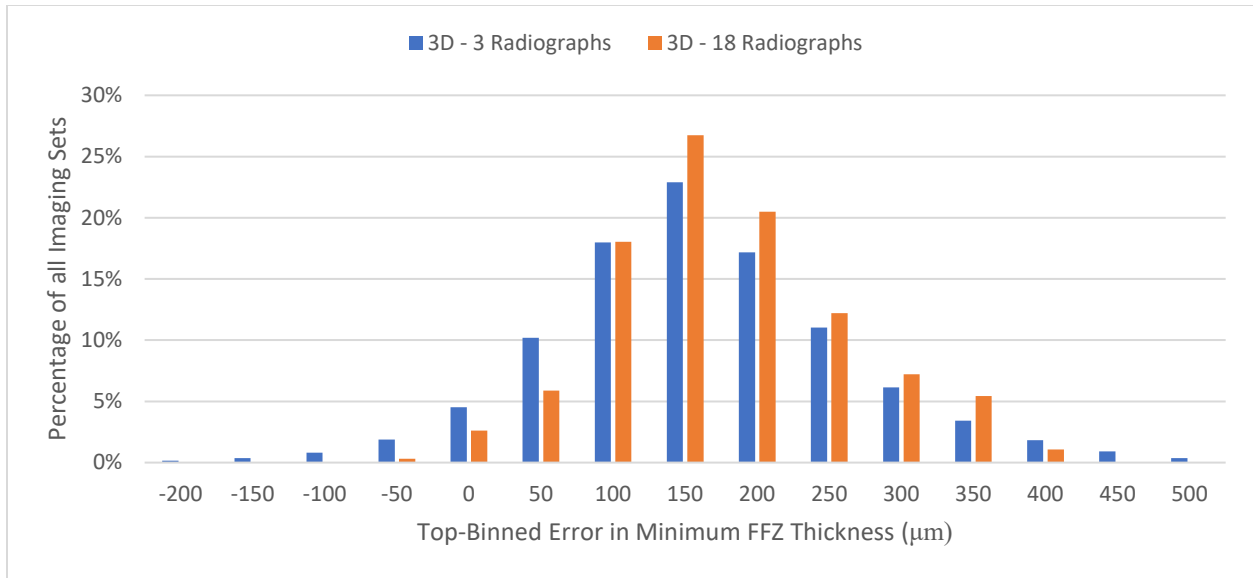


Fig. 6. Distribution of error in minimum fuel-free zone thickness across all imaging sets tested for both 3 and 18 radiographs distributed in 3D per image set.

In contrast to the mean fuel-free zone thickness, the error in the calculated minimum fuel-free zone thickness was biased in the positive direction, as shown in the distribution of error for two imaging strategies in **Fig. 6**. Again, this behavior arose naturally from the fuel core ellipsoid fitting process, as the best fit will tend to undercut the fuel core points which are the furthest out from the core and thus closest to the pebble surface. Unfortunately, this bias works against the general objective of identifying pebbles with an insufficiently thick fuel-free zone. Based on the mean and standard deviation of the error in minimum fuel-free zone thickness, an upper limit of uncertainty may be calculated as shown in **Fig. 7**. As with the error in the mean fuel-free zone thickness, the mean and standard deviation of the error in the minimum fuel-free zone thickness decreased with an increasing number of radiographs per imaging set and did not change significantly between the planar and the 3D distribution of radiographs.

becomes, until the particles are only visible at the exact angle in which they are orthogonal to the source/detector axis. This results in rapidly diminishing returns in the probability of capturing particles in the fuel-free zone (equivalent to the percentage of FFZ imaged) as additional images are added to the 2D fixed angle strategy, as shown in **Fig. 8**. For this analysis, each of the 100 randomly generated digital pebbles described in Section 2.1 was rotated to hundreds of different angles to simulate loading in random orientations. Sets that included between three and sixty evenly spaced digital radiographs of each pebble/orientation combination were created as described in Section 2.2, and voxels within the fuel-free zone which were not occluded by the fuel core were tallied.

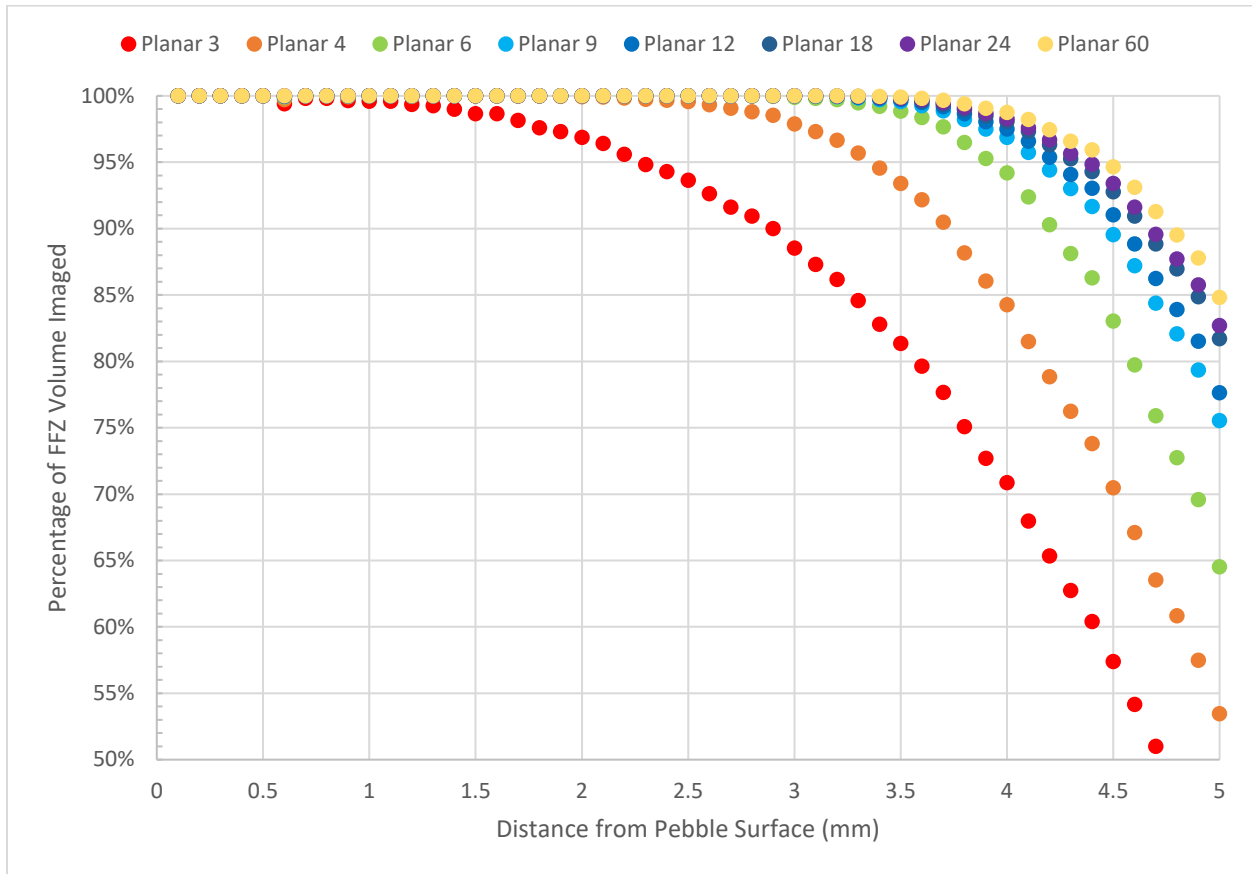


Fig. 8. Percentage of FFZ imaged as a function of distance from the pebble’s surface for various numbers of planar radiographs of randomly generated digital pebbles.

Increasing the number of planar images acquired initially results in significant gains in probability of finding escaped particles at a given depth. For example, doubling from three to six radiographs per image set improves the probability of finding a particle at 4 mm from the pebble surface from 71 to 94%. However, diminishing returns rapidly constrain further improvement, as increasing the number of radiographs by an additional factor of ten results in an improvement to only 99%. This effect is shown schematically in **Fig. 9**. As additional radiographs are acquired, blind spots within the fuel-free zone are initially reduced substantially; however, as more radiographs are added, the amount of overlap with prior radiographs increases (shown by progression from orange to yellow), and the reduction in blind spots decreases. Note that due to the random variations in fuel core shapes introduced in Section 2.1, the results in **Fig. 8** do not exactly match the geometric progression implied by the simplified schematic in **Fig. 9**.

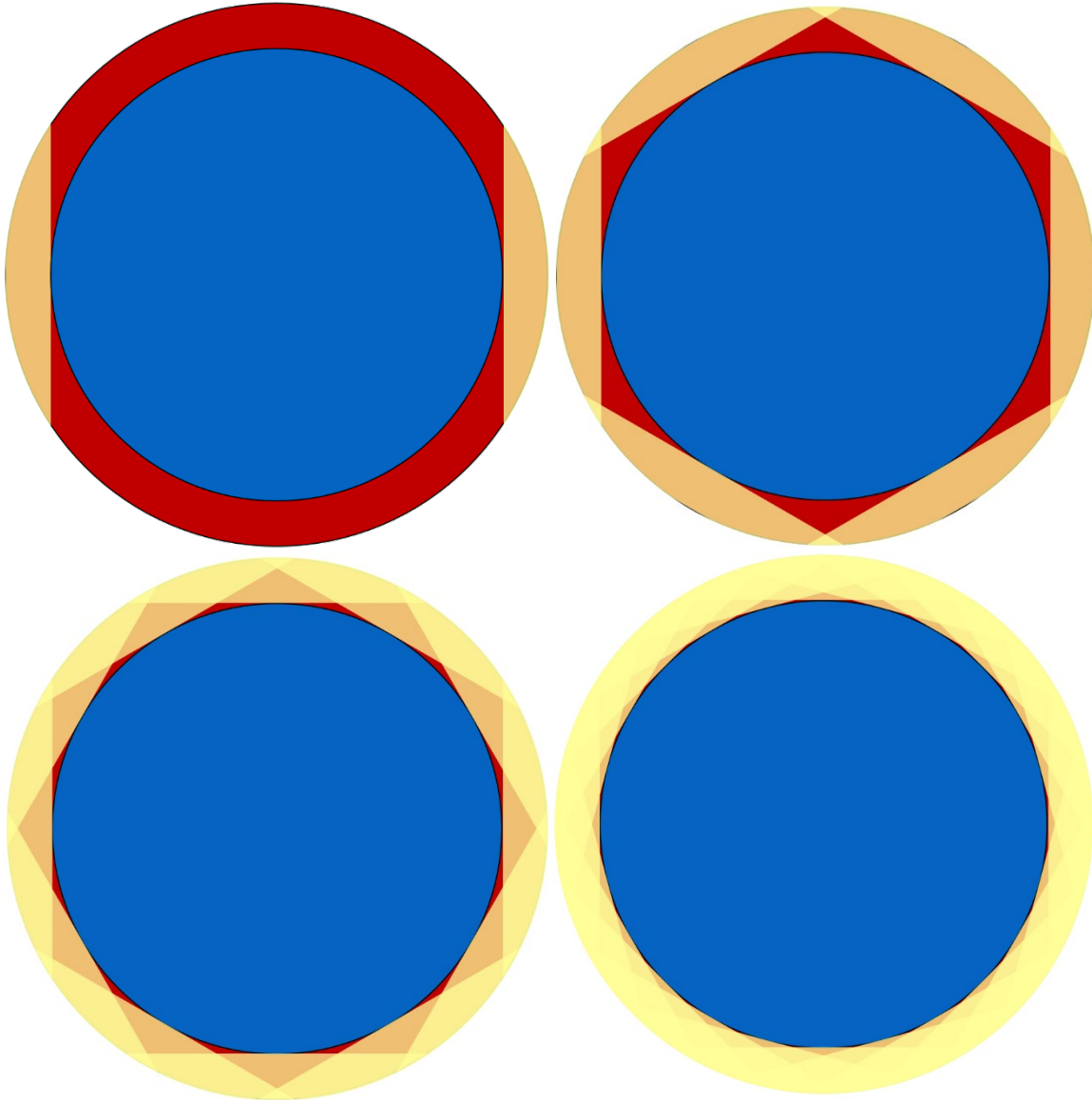


Fig. 9. Top-down view of blind spots (red) due to the fuel core (blue) within the fuel-free zone after one, three, six, and twelve evenly distributed planar radiographs (yellow).

4.2 3D Fixed Angle Strategy

Design of a pebble radiography system which allows for imaging from any angle in 3D is more challenging than the base case of 2D rotation; however, the problem of diminishing returns with additional images is significantly reduced. The same set of 100 randomly generated pebbles rotated to hundreds of different angles used in Section 4.1 was used again to test a 3D fixed angle strategy, but in this case, sets of between three and thirty imaging angles were evenly distributed in 3D. Determination of 3D angular distributions corresponding to platonic solids was straightforward based on known geometry, but for higher numbers of images there is no perfect distribution of evenly spaced angles in 3D space. In these cases, approximately evenly spaced distributions of angles were generated by starting with a random distribution of angles, then allowing each angular point to shift based on repulsion to nearby points until a stable set of well-distributed angles were obtained. As shown in **Fig. 10**, diminishing returns in the percentage of particles caught

(equivalent to the percentage of FFZ imaged) with increasing numbers of radiographs are still present, particularly near the fuel core. However, removal of the restriction of imaging angles to a single plane results in much greater efficiency for higher numbers of radiographs.

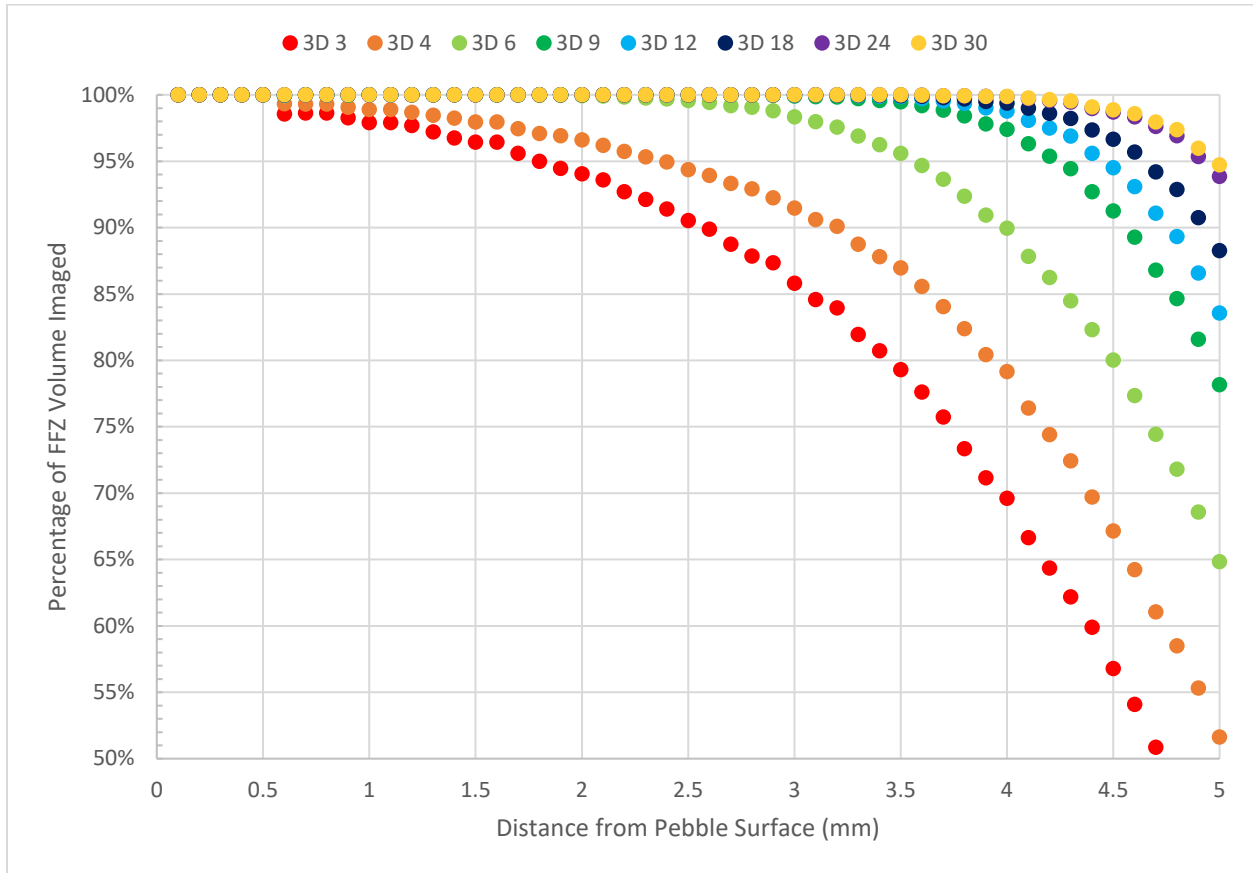


Fig. 10. Percentage of FFZ volume imaged as a function of distance from the pebble surface for various numbers of 3D distributed radiographs of randomly generated digital pebbles.

The 2D and 3D fixed angle strategies may be compared based on the probability of finding escaped particles at a given critical depth from the pebble surface. As shown in **Fig. 11**, for the dataset considered, the planar strategy was more effective in identifying escapees at a depth of 4 mm from the pebble surface for smaller radiograph sets of less than nine radiographs per pebble, while the 3D strategy was more effective for larger radiograph sets. The selection of a 4 mm depth for comparison is arbitrary, as the critical zone depth for a given design will depend on reactor design.

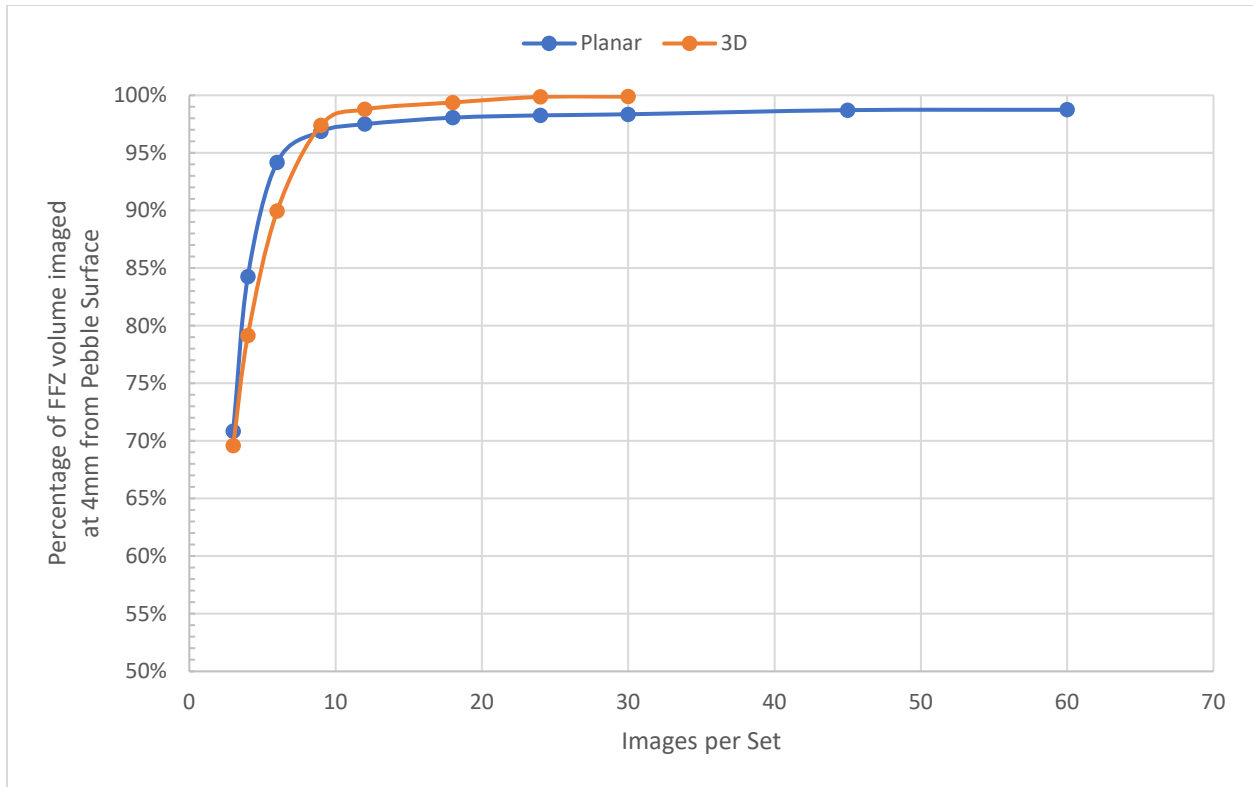


Fig. 11. Comparison of the effectiveness of planar and 3D fixed angle strategies for imaging the FFZ at a depth of 4 mm from the pebble surface.

4.3 Adaptive Radiograph Strategies

The fixed angle strategies considered in Sections 4.1 and 4.2 treat every pebble identically, both in terms of the number of radiographs acquired and their spacing. While this approach is straightforward, it is not efficient. Pebbles with smaller, well-centered fuel cores will generally require fewer radiographs to establish the absence of escaped particles at a given depth due to reduced occlusion of the fuel-free zone by the fuel core. In addition, variations in fuel core shape and centering will change the relative value of different imaging angles in terms of revealing potential escapees. Thus, the number of radiographs required to achieve a given level of certainty for catching particles at a given depth may be significantly reduced by employing an adaptive strategy which continuously evaluates the highest value angle for each additional radiograph based on the data already acquired. This adaptive strategy may be applied in either 2D or 3D imaging freedom, but only the 2D case is covered herein, as it was found to be efficient enough that the additional effort of imaging with an extra axis of rotation was deemed unnecessary.

For the 2D adaptive strategy, a simple algorithm was created which evaluates a set of pebble radiographs to identify the point nearest to the pebble surface which has not yet been imaged without occlusion by the fuel core. The angle of the next radiograph was chosen such that the line from the pebble centroid to that point was perpendicular to the imaging direction. This process was repeated until either the entire fuel-free zone up to a given depth from the surface was imaged without occlusion by the fuel core, or a particle was found within that given depth. While the algorithm employed was relatively simple, it has the advantage of being very fast, requiring less than a second to run on a desktop computer. As such, implementation of this algorithm in a real system would not be expected to significantly increase the time required per radiograph.

The 2D adaptive strategy was applied to the same 100 randomly generated pebbles used in the work described in Sections 4.1 and 4.2 with 50 different starting rotations for each pebble to simulate randomly oriented loading. The critical fuel-free depth was set to be 4 mm from the pebble surface and a pebble was considered to have failed if any particles were found within that depth. Again, this critical depth is arbitrary, as the true value will vary with reactor design.

For every loading angle of every pebble, the algorithm either correctly identified a particle within the 4 mm critical depth from the pebble surface, or it successfully imaged the entirety of the fuel-free zone to a depth of 4 mm without occlusion by the fuel core. For the 35 pebbles with no particles within 4 mm of the surface, an average of 11.9 radiographs were required to fully image the fuel-free zone. Similarly, for the 65 pebbles with particles within 4 mm of the surface, an average of only 2.1 radiographs were required to identify an offending particle. For comparison, 2D fixed angle strategy with 12 radiographs provided a 97% confidence of catching particles within the critical depth, while the 3D fixed angle strategy with 12 radiographs provided a 99% confidence. Thus, in the nominal case of a pebble within specification, the adaptive strategy provides a higher confidence (100%) for the same number of radiographs. Although the absolute gain in terms of confidence is only a few percent, the long tail of confidence in finding particles within the critical zone as a function of the number of radiographs acquired as shown in **Fig. 11** make this small gain highly significant. This is shown in **Fig. 12** with the comparison of each method in imaging an example pebble. While the adaptive method converges to 100% confidence of no particles at the given depth in 10 radiographs, the fixed methods require 30 radiographs to reach 99.8% confidence (2D fixed) or 99.999% confidence (3D fixed).

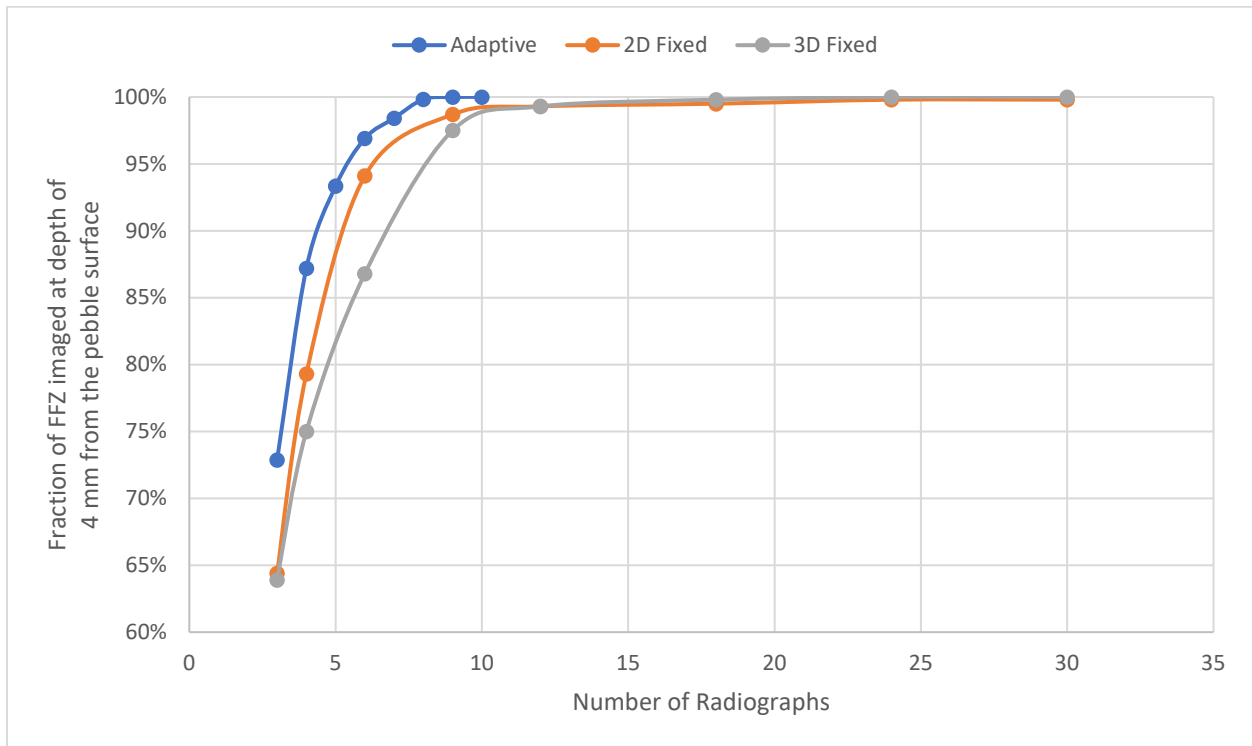


Fig. 12. Comparison of the effectiveness of the 2D adaptive method to fixed methods in imaging the fuel-free zone at a given depth from the pebble surface.

5 Testing with Actual Pebble XCT Datasets

The adaptive imaging strategy developed using simulated radiography was tested using XCT datasets for two actual pebbles. One of these pebbles represented the typical case of a relatively uniform fuel-free zone thickness around the pebble with no escaped particles, while the other represented the undesirable case of a pebble with escaped particles. Both pebbles were imaged using a Zeiss Versa 520 with the source set to 100 kV and 8 W, 3201 radiographs over 360° per image set, and a voxel size of 55 μm . Image analysis of the first pebble with no escaped particle found a minimum fuel-free zone thickness of 4.65 mm. As shown in **Fig. 13**, there were two escaped particles in this pebble, one near the surface and one midway through the fuel-free zone.

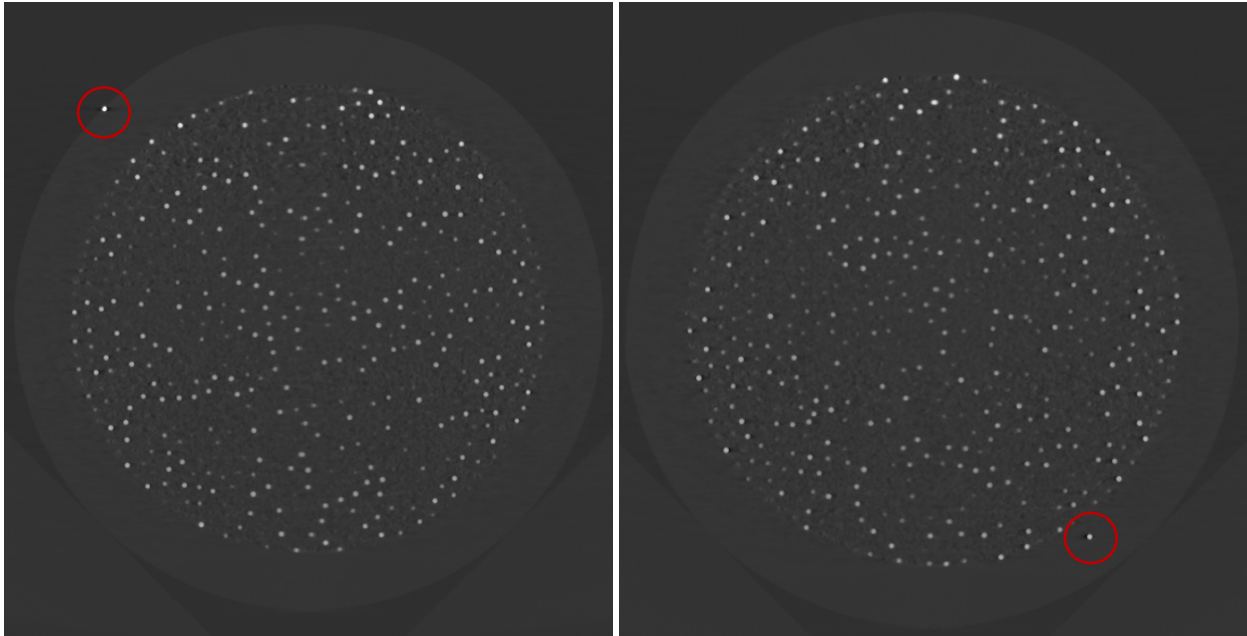


Fig. 13. Radiographs of second pebble showing escaped particles near the pebble surface (left) and midway through the fuel-free zone (right)

The adaptive radiography strategy was applied to each pebble by selecting a starting angle for the first image and calculating following target angles based on the cumulative radiography results. Radiographs for each target angle were taken from the set of 3201 radiographs taken of each pebble by finding the nearest actual radiograph angle. A total of 24 starting angles evenly distributed over 360° were tested for each pebble to test the effect of different starting positions. Both pebbles were tested with critical depths between 4.00-4.75 mm.

Under these conditions, the pebble with two escapee particles was correctly “failed” in every case, typically in just a few radiographs. The pebble without any escapee particles and a true minimum fuel-free zone thickness of 4.65 mm correctly “passed” in every case with a critical depth between 4.00-4.5 mm and correctly “failed” in every case with a critical depth of 4.75 mm, with results for the number of radiographs required given in **Table 2**. The required number of radiographs to pass or fail for each critical depth increased with increasing critical depth due to the increasing impact of occlusion by the fueled region.

Table 2. Required number of radiographs to pass or fail test pebble with no escaped particles and a true minimum fuel-free zone thickness of 4.65 mm.

Critical Depth	Result	Number of Radiographs		
		Minimum	Mean	Maximum
4.00	Passed	6	7.3	8
4.25	Passed	8	8.5	10
4.50	Passed	10	11.8	13
4.75	Failed	10	12.2	16

The progress of the algorithm after each radiograph may be tracked either by considering the minimum blind spot depth from the pebble surface or by considering the remaining volume within the critical depth to be imaged. As shown in **Fig 14**, the minimum blind spot depth follows an s-curve pattern. The first few radiographs have no impact on blind spot depth due to not fully imaging the pebble surface, but once the pebble surface is fully imaged the minimum blind spot depth quickly increases with additional radiographs before diminishing returns set in with the final few radiographs required to surpass the critical depth threshold.

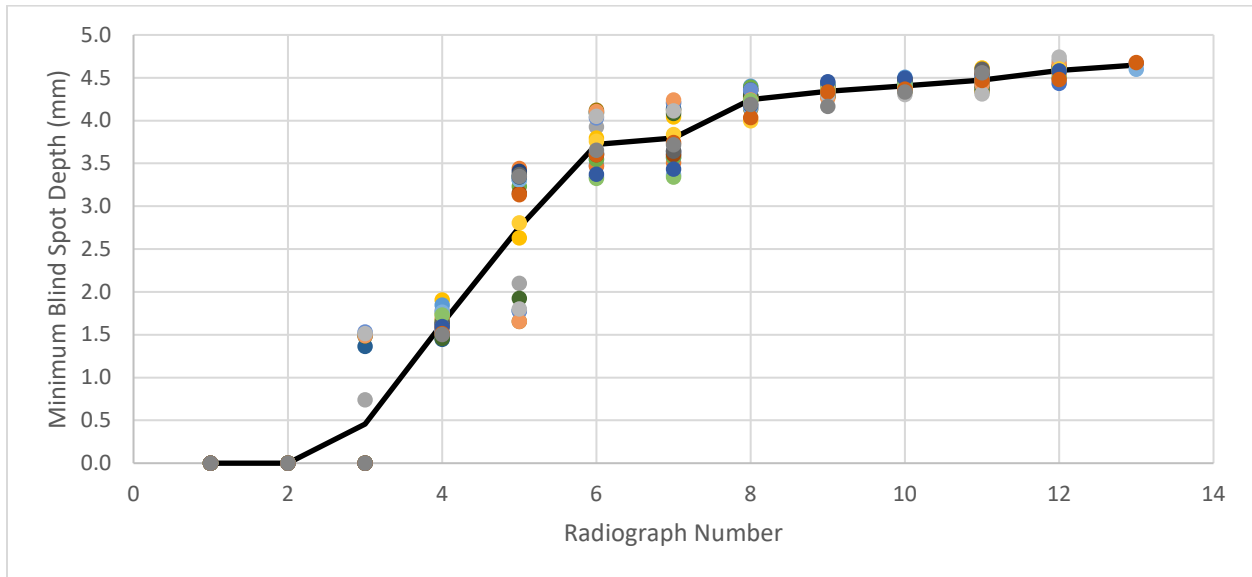


Fig 14. Minimum blind spot depth as a function of radiograph number for the pebble with no escaped particle and a critical depth of 4.5 mm. The mean value across all starting angles is shown as a solid line.

Viewed on a logarithmic scale as in **Fig. 15**, the remaining fraction of the fuel-free zone within the critical depth to be imaged decreases steadily with each additional radiograph. The additional fraction imaged with each additional radiograph is initially very similar for the various critical depths tested, but as the number of radiographs increases the higher critical depths begin to lag behind. This effect is due to the increasing challenge of imaging regions very close to the fuel core surface, as shown schematically in **Fig. 9**.

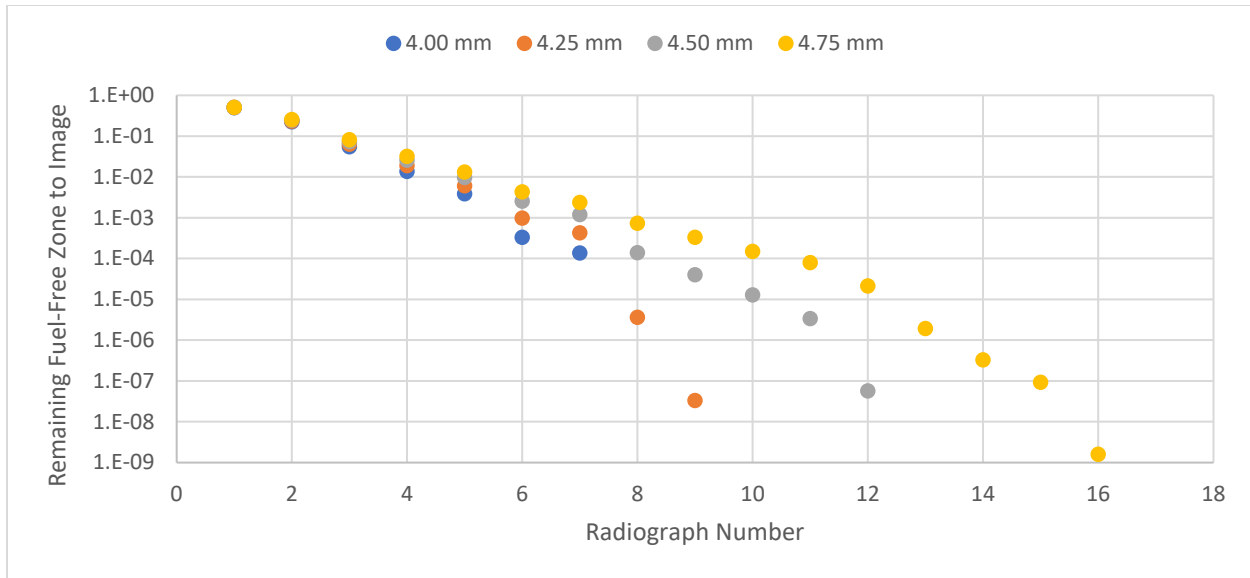


Fig. 15. Mean remaining fraction of designated fuel-free zone to be imaged after each radiograph for various critical depths for the pebble with no escaped particles.

6 Conclusions

A method for generating digital analogs of TRISO-bearing nuclear fuel pebbles and simulating their radiographs was developed to rapidly test the effectiveness of different imaging strategies for measuring variations in fuel-free zone thickness and identifying pebbles with TRISO particles within the fuel-free zone. It was found that accurate ellipsoid models of the fuel core could be formed by projection of points on the fuel core surface from 2D radiographs into 3D and that these models could be used to estimate the uncertainty in the mean and minimum fuel-free zone thickness for pebbles. In the more complicated case of identifying particles within a critical depth from the pebble surface, fixed imaging strategies in 2D and 3D and an adaptive imaging strategy in two dimensions were tested. It was found that for fixed angle strategies the additional perspective allowed by the 3D imaging strategies resulted in significantly more rapid gains in confidence of catching particles within the critical zone as more images were taken. However, the 2D adaptive strategy was even more efficient thanks to its use of live feedback from internal models of the fuel core during imaging. The 2D adaptive strategy was successfully tested on two actual pebble XCT datasets across a range of starting positions and critical depths. In every case the algorithm correctly identified whether the pebble should pass or fail in a relatively modest number of radiographs.

Data Availability

The raw/processed data required to reproduce these findings cannot be shared at this time due to technical or time limitations.

Acknowledgements

This work was sponsored by the U.S. Department of Energy, Office of Nuclear Energy, through the Advanced Reactor Concepts ARC-Xe program.

7 References

- [1] P. Demkowicz, B. Liu and J. Hunn, "Coated particle fuel: Historical perspectives and current progress," *Journal of Nuclear Materials*, vol. 515, pp. 434-450, 2019.
- [2] H. Nabielek, G. Kaiser, H. Huschka, H. Ragoss and M. T. W. Wimmers, "Fuel for pebble-bed HTRs," *Nuclear Engineering and Design*, vol. 78, pp. 155-166, 1984.
- [3] G. Helmreich, J. Hunn, D. Brown and B. Blamer, "New method for analysis of x-ray computed tomography scans of TRISO fuel forms," *Nuclear Engineering and Design*, vol. 357, 2020.
- [4] L. Zhu, X. Xiang, Y. Du, G. Yu, Z. Li, Y. Peng and X. Wang, "Uniformity Assessment of TRISO Fuel Particle Distribution in Spherical HTGR Fuel Element Using Voronoi Tessellation and Delaunay Triangulation," *Science and Technology of Nuclear Installations*, vol. 2018, 2018.
- [5] G. Yu, Y. Du, X. Xiang, Y. Liu, Z. Li and X. Wang, "3D Nondestructive Visualization and Evaluation of TRISO Particles Distribution in HTGR Fuel Pebbles Using Cone-Beam Computed Tomography," *Science and Technology of Nuclear Installations*, vol. 2017, 2017.
- [6] P. Hania, B. Janssen, A. Fedorov, S. Knol, S. deGroot, M. L. A. van de Sande and M. Futterer, "Qualification of HTR pebbles by X-ray tomography and thermal analysis," *Nuclear Engineering and Design*, vol. 251, pp. 47-52, 2012.
- [7] A. Kercher and J. Hunn, "Statistical methods for Material Characterization and Qualification ORNL/TM-2005/542," Oak Ridge National Laboratory, Oak Ridge, Tennessee, 2005.
- [8] A. Thompson, I. Maskery and R. Leach, "X-ray computed tomography for additive manufacturing: a review," *Measurement Science and Technology*, vol. 27, no. 7, 2016.
- [9] G. Yu, Y. Du, X. Xiang, Y. Liu, Z. Li and X. Wang, "3D Nondestructive Visualization and Evaluation of TRISO Particles Distribution in HTGR Fuel Pebbles Using Cone-Beam Computed Tomography," *Science and Technology of Nuclear Installations*, 2017.
- [10] Y. Du, X. Wang, X. Xiang and B. Liu, "Automatic x-ray inspection for the HTR_PM spherical fuel elements," *Nuclear Engineering and Design*, vol. 280, pp. 144-149, 2014.
- [11] M. Yang, R. D. J. Li, L. Liang, X. Li, W. Liu and F. Meng, "Analysis of DR testing blind zone of spherical fuel elements for 10 MW high-temperature gas-cooled reactor," *NDT&E International*, vol. 60, pp. 77-86, 2013.
- [12] X. Zhao, Y. Peng, X. Wang, L. Zhu and H. Chen, "Spatial Uniformity Assessment of Particles Distributed in a Spherical Fuel Element Using a Non-Destructive Approach," *Scientific Reports*, vol. 9, 2019.